nature physics
LETTERS
PUBLISHED ONLINE: 12 JUNE 2011 | DOI: 10.1038/NPHYS2008

Quantum Hall effect and Landau-level crossing of Dirac fermions in trilayer graphene

Thiti Taychatanapat[1], Kenji Watanabe[2], Takashi Taniguchi[2] and Pablo Jarillo-Herrero[3]*

The physics of Dirac fermions in condensed-matter systems has received extraordinary attention following the discoveries of two new types of quantum Hall effect in single-layer and bilayer graphene[1–3]. The electronic structure of trilayer graphene (TLG) has been predicted to consist of both massless single-layer-graphene-like and massive bilayer-graphene-like Dirac subbands[4–7], which should result in new types of mesoscopic and quantum Hall phenomena. However, the low mobility exhibited by TLG devices on conventional substrates has led to few experimental studies[8,9]. Here we investigate electronic transport in high-mobility (>100,000 $cm^2 V^{-1} s^{-1}$) TLG devices on hexagonal boron nitride, which enables the observation of Shubnikov–de Haas oscillations and an unconventional quantum Hall effect. The massless and massive characters of the TLG subbands lead to a set of Landau-level crossings, whose magnetic-field and filling-factor coordinates enable the determination of the Slonczewski–Weiss–McClure (SWMcC) parameters[10] used to describe the peculiar electronic structure of TLG. Moreover, at high magnetic fields, the degenerate crossing points split into manifolds, indicating the existence of broken-symmetry quantum Hall states.

Bernal- or ABA-stacked TLG (Fig. 1b) is an intriguing material to study Dirac physics and the quantum Hall effect (QHE) because of its unique band structure, which, in the simplest approximation, consists of massless single-layer-graphene (SLG)-like and massive bilayer graphene (BLG)-like subbands at low energy (Fig. 1c; refs 4–7). The energies of the Landau levels (LLs) for massless charge carriers depend on the square root of the magnetic field $\sqrt{B}$ (refs 1, 2,11–13), whereas for massive charge carriers they depend linearly on B (refs 3,11,12,14). Therefore, the LLs from these two different subbands in TLG should cross at some finite fields, resulting in accidental LL degeneracies at the crossing points. However, one of the main challenges so far to observe the QHE in TLG has been its low mobility on SiO_2 substrates[8,9]. To overcome this problem, we use hexagonal boron nitride (hBN) single crystals[15] as local substrates, which have been shown to reduce carrier scattering in graphene devices[16] (See Methods and Supplementary Information for fabrication). Substrate-supported devices also enable us to reach higher carrier density than suspended samples[17], which is necessary for the observation of the LL crossings.

Figure 1e,f shows the resistivity and conductivity of a TLG device at zero magnetic field. The resistivity at the Dirac peak exhibits a strong temperature dependence, which in SLG is a strong indication of high device quality[18,19]. In addition, we also observe a double-peak structure at low temperatures (Fig. 1e). This double-peak structure is probably due to the band overlap that occurs in TLG when all SWMcC parameters are included in the tight-binding calculation of its band structure, as we show below. The field-effect mobility of this device reaches 110,000 $cm^2 V^{-1} s^{-1}$ at 300 mK at densities as high as 6×10^{11} cm^{-2}. This mobility value is two orders of magnitude higher than previously reported values for supported TLG (refs 8,9) and comparable to suspended samples[17,19]. The low disorder and high mobility enable us to probe LL crossings of Dirac fermions through the measurement of Shubnikov–de Haas oscillations (SdHOs).

Figure 2a shows longitudinal resistivity ρ_{xx} as a function of $1/B$, for a carrier density $n=-4.4\times10^{12}$ cm^{-2}. At low B (below ~1 T), there are a number of oscillations characterized by broad minima separated by relatively narrower maxima. Beyond ~1 T, the minima become sets of narrower oscillations, and a clear pattern emerges: each minimum in the oscillations indicates a completely filled LL with corresponding filling factor $\nu = hn/eB$, where h is Planck's constant, and e is the electron charge. Within a single-particle picture, each LL is fourfold degenerate, the degeneracy originating from the valley and spin degrees of freedom in both the SLG-like and BLG-like subbands. When LLs from these two subbands cross at a given B, the coexistence of two fourfold degenerate LLs increases the degeneracy to eightfold. This eightfold degeneracy is highlighted by the green bands in Fig. 2a, where ν changes by 8 from one minimum to the next instead of by 4. For $B \geq 4$ T, the splitting of the LLs results in ν changing by either 1 or 2, as the different broken-symmetry quantum Hall states are occupied.

A more complete understanding of the TLG LL energy spectrum is obtained by plotting ρ_{xx} as a function of n and B (Fig. 2b). The resulting fan diagram lines correspond to the SdHOs, whereas the white central region corresponds to an insulating behaviour at $\nu = 0$ (see Supplementary Information). The above-mentioned crossings of SLG-like and BLG-like LLs manifest themselves as a beating pattern in the SdHOs, with a greater number of them and more visible on the hole side ($n < 0$). This electron–hole asymmetry results from the TLG band structure, as we show below. In addition, the LL splittings appear as finer split lines in the SdHOs. For each LL crossing, there is an enhancement of ρ_{xx} due to the enhanced density of states[20,21], and each crossing point can be uniquely identified by B and ν.

The positions of the crossings in B and ν space depend sensitively on the TLG band structure, and therefore enable an electronic-transport determination of the relevant SWMcC parameters for TLG. These parameters, proposed to explain the band structure of graphite[10], describe the different intra- and interlayer hopping terms in the different graphene sheets (Fig. 1b). The simplest TLG model, in which only the nearest intra- and interlayer couplings (γ_0 and γ_1) are considered, results in symmetric electron and hole bands (Fig. 1c) and therefore is clearly insufficient to explain the experimental data. We therefore use all the relevant SWMcC parameters to numerically calculate the LL energy spectrum (Fig. 2c) and density of states as a function of B (Fig. 2d), and carry out a minimization procedure to fit the experimental

[1]Department of Physics, Harvard University, Cambridge, Massachusetts 02138, USA, [2]National Institute for Materials Science, Namiki 1-1, Tsukuba, Ibaraki 305-0044, Japan, [3]Department of Physics, Massachusetts Institute of Technology, Cambridge, Massachusetts 02139, USA. *e-mail: pjarillo@mit.edu.

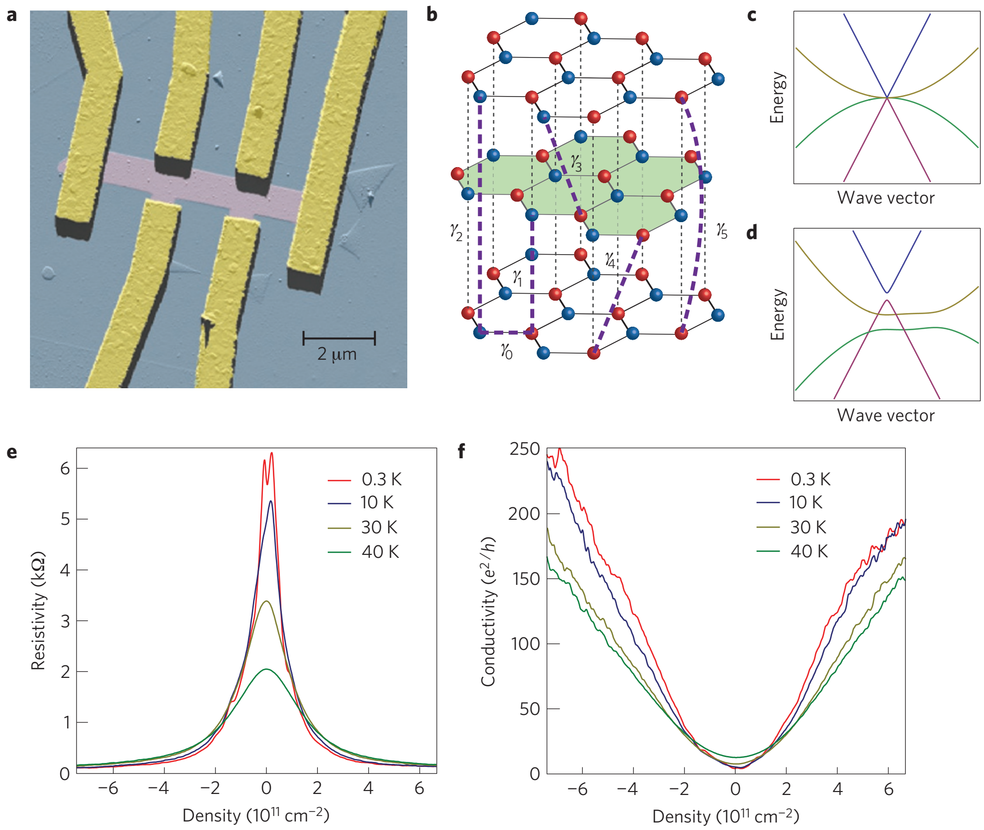

Figure 1 | Electronic properties of Bernal-stacked TLG at zero magnetic field. a, False-colour atomic force microscopy image of a TLG Hall-bar device on hBN. **b**, Bernal-stacked TLG atomic lattice. The SWMcC hopping parameters, γ_i, are shown by purple dashed lines connecting the corresponding hopping sites. In addition to γ_i, the SWMcC parameters also include the on-site energy difference, δ, between A and B sublattices (blue and red lattices). **c**, Band structure of TLG at low energy, which takes into account only the nearest-neighbour intra- and interlayer hopping parameters γ_0 and γ_1. **d**, Band structure of TLG within a full-parameter model, with the parameters calculated from the SdHOs in Fig. 2b. **e**, Resistivity as a function of density and temperature for TLG. The double-peak structure starts to emerge as temperature decreases below 10 K. **f**, Conductivity as a function of density and temperature. The field-effect mobility reaches ~110,000 cm^2 V^{-1} s^{-1} at 300 mK and decreases to ~65,000 cm^2 V^{-1} s^{-1} at 40 K.

data in Fig. 2b. To reduce the number of parameters, we take $\gamma_0 = 3.1$ eV, $\gamma_1 = 0.39$ eV and $\gamma_3 = 0.315$ eV (see Supplementary Information), and we obtain from our fit the following values of the SWMcC parameters: $\gamma_2 = -0.028(4)$ eV, $\gamma_4 = 0.041(10)$ eV, $\gamma_5 = 0.05(2)$ eV, and $\delta = 0.046(10)$ eV. The definitions of the γ_i can be found in Fig. 1b and δ is the on-site energy difference between the two inequivalent carbon sublattices residing in the same graphene layer. The values of the SWMcC parameters obtained are similar to previously reported values for graphite[10] and, apart from the broken-symmetry states (see discussion below), our data agree very well with the LLs corresponding to Bernal-stacked TLG, and not to rhombohedral-stacked TLG (ref. 22). These parameters result in the overall electron–hole asymmetric band structure shown in Fig. 1d, with small bandgaps $E_{g,S} \sim 7$ meV and $E_{g,B} \sim 14$ meV for the SLG- and BLG-like subbands, and a band overlap $E_o \sim 14$ meV.

The LLs in TLG are not truly fourfold degenerate even in a single-particle picture, owing to the finite values of γ_2, γ_5 and δ, which break valley degeneracy[23] (Fig. 2c), in addition to the Zeeman interaction, which breaks spin degeneracy. Our data at high B (Fig. 2a,b) show that the splitting of fourfold-degenerate LLs is observed up to filling factors as high as $\nu = 46$. Whereas single-particle effects may partly explain these broken-symmetry quantum Hall states (for example, from the width of the LL crossings, we estimate the disorder broadening of the LLs to be ~1 mV, similar to the Zeeman splitting at ~8 T), it is likely that electron–electron interactions play a significant role too, as is the case in SLG and BLG (refs 16,24–27). For example, the insulating behaviour we observe at $\nu = 0$ cannot be explained by single-particle effects, given the band overlap between the SLG- and BLG-like subbands, and the single-particle LL energy spectrum shown in Fig. 2c. Figure 2e shows example traces where the different behaviour of LL crossings and LL splitting can be seen.

At high B, the LL crossing points should become crossing manifolds owing to the crossing between the split SLG- and BLG-like LLs. One such example is shown in Fig. 3a. From the LL energy spectrum shown in Fig. 2c, the manifold corresponds to the crossing between the $N = -1$ LL of the SLG-like subband, LL_S^{-1}, and the $N = -5$ LL of the BLG-like subband, LL_B^{-5}. To reproduce the observed degeneracies at the crossings, the fourfold LL_S^{-1} has to completely split into four singly degenerate LLs whereas the fourfold LL_B^{-5} splits into three LLs: two singly degenerate LLs and one doubly degenerate LL. Figure 3b shows schematically the full 12-point manifold, of which only six crossing points are visible in our density and magnetic-field range. We have found that this splitting scheme is the only one that yields the correct result for both the degeneracies at the crossings and the filling factors at which they occur. The observation of the full fourfold splitting of the LL_S^{-1} in TLG, although expected, is remarkable because previous transport studies of the $N = 1$ LL in SLG had reported only the breaking of some of the degeneracies[24,28], and the full fourfold splitting has only been seen in recent STM experiments[29]. The 1–2–1 splitting of LLs from the BLG-like subband, however, is more anomalous. Naively, we would expect the splitting to be either twofold or fourfold, depending on whether either valley or spin is split or both are[26,27].

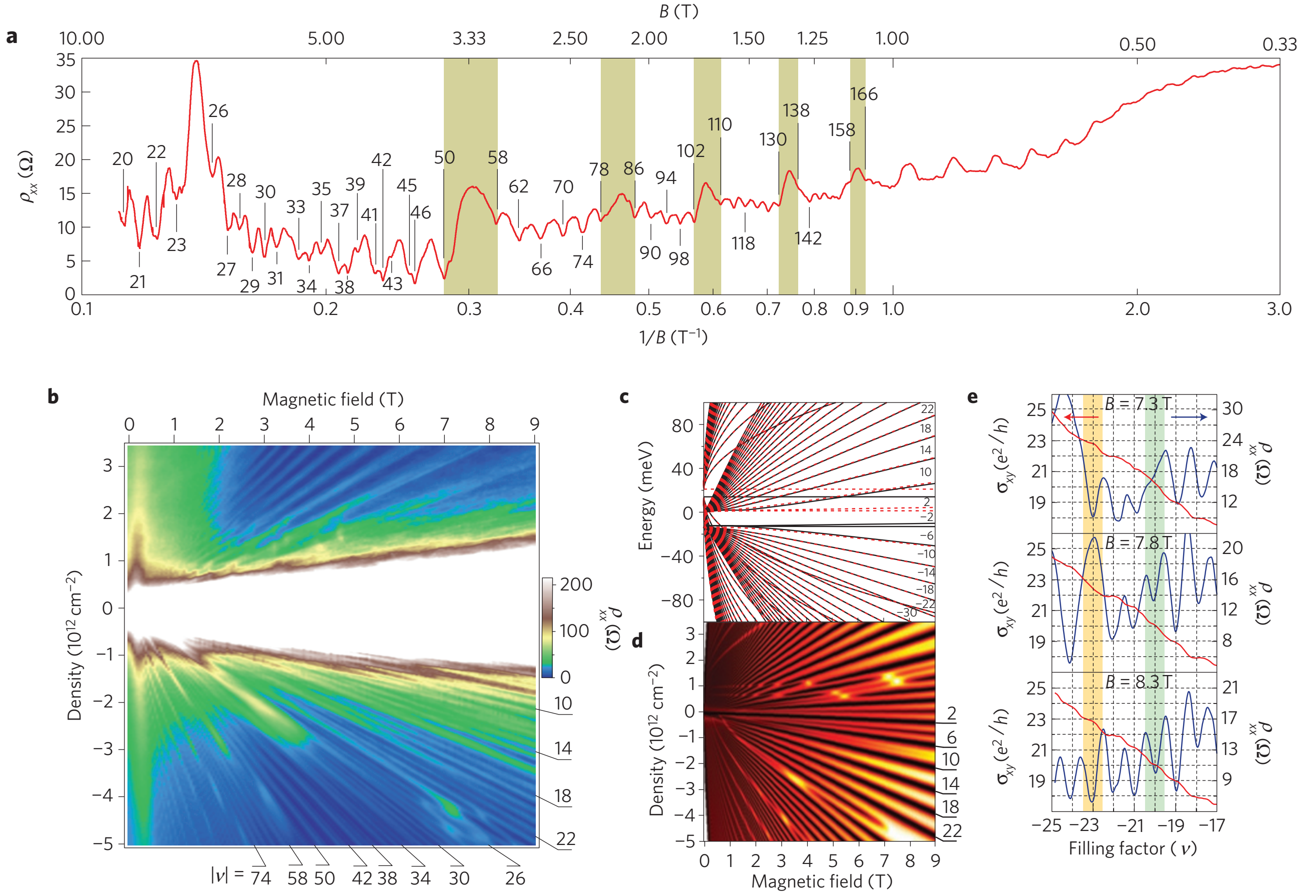

Figure 2 | SdHOs and Landau fan diagram in TLG. a, ρ_{xx} as a function of inverse magnetic field at 300 mK. The numbers inside the figure indicate the filling factors at the SdHO minima. The highlighted bands show the regions of eightfold degeneracy, which provide evidence for LL crossings of the SLG- and BLG-like subbands. For $B > 4$ T, the SdHO minima are separated by $\Delta\nu = 1$ or 2, indicating the splitting of LLs. **b**, Colour map of ρ_{xx} versus n and B at 300 mK. The diagonal lines correspond to constant-filling-factor lines. The beating pattern, most visible at negative densities, is a consequence of LL crossings. The white central region corresponds to an insulating state at zero density (see Supplementary Information). **c**, Calculated LL energy spectrum in TLG for the SWMcC parameters obtained from **b**. The red dashed and black lines are LLs at K and K′ points respectively. The roughly $\sqrt{B}$-like and linear B-like dispersion from the SLG- and BLG-like subbands is evident. Each line corresponds to a spin-degenerate LL. **d**, Calculated density of states as a function of density and magnetic field from the LL spectrum in **c**. Apart from the LL splitting, the location of the LL crossings agrees very well with the experimental data in **b**. **e**, ρ_{xx} and σ_{xy} as a function of filling factor for $B = 7.3, 7.8$ and 8.3 T. The highlighted orange region shows the appearance of the LL crossing at $\nu = -23$ whereas the green highlighted region shows the LL splitting occurring at $\nu = -20$.

However, we note that this 1–2–1 splitting may also be present in a recent study of BLG on hBN in the intermediate-B regime[16], and may possibly indicate a richer phase diagram based on SU(4) rather than SU(2) × SU(2) symmetry breaking. A detailed study of the crossing between spin/valley-polarized LLs of massless and massive Dirac fermions, together with the possible role of electron–electron interactions, could potentially lead to some intriguing phenomena such as phase transitions in quantum Hall ferromagnets[20,30].

Although the splitting of the LLs at high B provides insight into broken symmetries in TLG in the quantum Hall regime, it also masks out the quantum Hall plateaus expected within the simplest single-particle model for TLG. The sequence of plateaus arising from such simple models has proven to be a useful tool in identifying SLG and BLG (refs 1–3). For completeness, Fig. 4 shows ρ_{xx} and Hall conductance σ_{xy} at $B = 9$ T before current annealing, that is, in the presence of increased disorder, which prevents the observation of LL splitting. In the simplest model, the QHE plateaus are expected at $\sigma_{xy} = \pm 4(N + 1/2 + 1)e^2/h$ for $N = 0, 1, \ldots$, where the 12-fold zero-energy LL results from the fourfold and eightfold zero-energy LLs of the SLG- and BLG-like subbands, respectively[31,32]. The observed plateaus at $\pm 10, \pm 14, \pm 18 e^2/h$ agree with this simple prediction, but we observe in addition extra plateaus for $\nu = \pm 2$ and ± 4 as well as the absence of a plateau at $\nu = +6$. This unconventional QHE can be explained within the band model calculated using the SWMcC parameters obtained from Fig. 2a–c. In such a model, the non-zero values of γ_2, γ_5 and δ lift the degeneracy of the 'zero-energy' LLs of the SLG- and BLG-like subbands (Fig. 2c). In addition, the fourfold-degenerate $N = 0$ LL of the SLG-like subband splits into two twofold-degenerate valley-polarized LLs, and the eightfold-degenerate (spin, valley and $N = 0, 1$ LLs) zero-energy LLs of the BLG-like subband splits into two fourfold-degenerate LLs (the splitting between $N = 0$ and $N = 1$ LLs remains relatively small compared with the valley splitting)[23]. We note that the Zeeman splitting is at least an order of magnitude smaller than other types of splitting even at 9 T, which is the reason why LLs remain spin degenerate in this non-interacting model.

The inset to Fig. 4 shows the calculated density of states as a function of energy at 9 T. The zero density is located between two nearly degenerate LLs, each with twofold degeneracy, which explains the observed plateaus at $\nu = \pm 2$. The absence of a plateau at $\nu = 0$ is probably due to disorder, which smears out the small energy gap between these two LLs. The plateaus at $\nu = \pm 4$ stem from the next twofold-degenerate LLs. However, these plateaus are not yet completely developed at 9 T, especially the one at $\nu = -4$

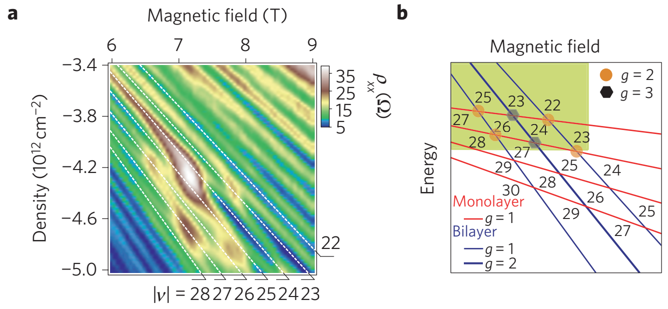

Figure 3 | LL crossings between broken-symmetry states. a, ρ_{xx} as a function of density and magnetic field at 300 mK showing a manifold of LL crossing points. The high-ρ_{xx} regions correspond to enhanced degeneracy due to LL crossings. Five crossing points are clearly visible and the sixth point is starting to appear in the lower right corner. White dashed lines are guides to the eye for each ν labelled on the edges. **b**, Schematic splitting and crossing of LLs yielding the manifold of crossings shown in **a**. Red and blue lines represent the split LL spectrum for the broken-symmetry quantum Hall states of the $N=-1$ LL from the SLG-like subband and the $N=-5$ LL from the BLG-like subband, respectively. The degeneracies for each level are $g=1$ for thin lines and $g=2$ for the thick line. The highlighted green area corresponds to the region observed in the data in **a**. The numbers inside each region show the corresponding filling factors.

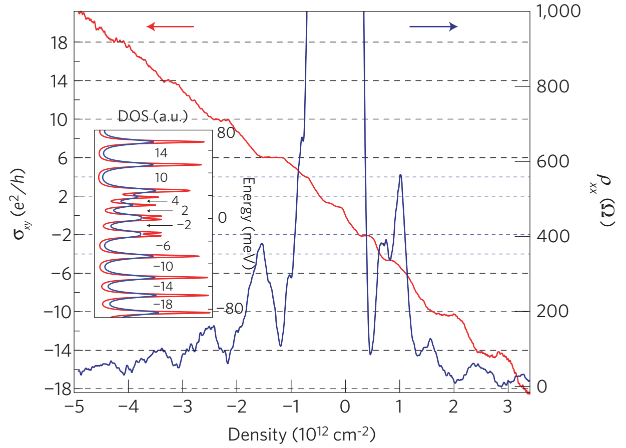

Figure 4 | Unconventional QHE in TLG. σ_{xy} and ρ_{xx} as a function of density at $B=9$ T and $T=300$ mK, and before the last current-annealing step. The long-dashed lines indicate the expected quantum Hall plateaus on the basis of the simplest TLG model approximation. The short-dashed lines indicate the extra quantum Hall plateaus based on the full band structure determined from Fig. 2c. Inset, Calculated density of states using the full SWMcC parameter model. The blue line is calculated using higher disorder broadening than the red line.

($\sigma_{xy}=4e^2/h$), which coincides with the small energy gap between this LL and the next one. Finally, the absence of a plateau at $\nu=+6$ ($\sigma_{xy}=-6e^2/h$) is due to the crossing between a twofold and a fourfold-degenerate LL. The degeneracy at the crossing becomes sixfold and causes the position of the plateau to step from $\nu=4$ to $\nu=10$ (the non-developed $\nu=4$ plateau does not reach its exact value at $\sigma_{xy}=-4e^2/h$). Unlike SLG and BLG, in which the sequence of the plateaus is the same for all B, the observed plateaus in TLG depend on B because of the LL crossing.

Methods

Figure 1a shows an atomic force microscope image of a Hall-bar-shaped TLG device on hBN. Our fabrication process consists of mechanically exfoliating hBN and graphene flakes on different supports, and a flip-chip bonding step to align them on top of each other (see Supplementary Information). The graphene flakes are then patterned into a Hall-bar geometry and contacted by electron-beam lithography. The device is then annealed in forming gas to remove residue and cooled down in a He-3 cryostat. To further reduce disorder, we carry out current annealing at low temperature[33].

Received 1 February 2011; accepted 21 April 2011; published online 12 June 2011

References

1. Novoselov, K. S. *et al.* Two-dimensional gas of massless Dirac fermions in graphene. *Nature* **438,** 197–200 (2005).
2. Zhang, Y., Tan, Y-W., Stormer, H. L. & Kim, P. Experimental observation of the quantum Hall effect and Berry's phase in graphene. *Nature* **438,** 201–204 (2005).
3. Novoselov, K. S. *et al.* Unconventional quantum Hall effect and Berry's phase of 2π in bilayer graphene. *Nature Phys.* **2,** 177–180 (2006).
4. Lu, C. L., Chang, C. P., Huang, Y. C., Chen, R. B. & Lin, M. L. Influence of an electric field on the optical properties of few-layer graphene with AB stacking. *Phys. Rev. B* **73,** 144427 (2006).
5. Guinea, F., Neto, A. H. C. & Peres, N. M. R. Electronic states and Landau levels in graphene stacks. *Phys. Rev. B* **73,** 245426 (2006).
6. Latil, S. & Henrard, L. Charge carriers in few-layer graphene films. *Phys. Rev. Lett.* **97,** 036803 (2006).
7. Partoens, B. & Peeters, F. M. From graphene to graphite: Electronic structure around the K point. *Phys. Rev. B* **74,** 075404 (2006).
8. Craciun, M. F. *et al.* Trilayer graphene is a semimetal with a gate-tunable band overlap. *Nature Nanotech.* **4,** 383–388 (2009).
9. Zhu, W., Perebeinos, V., Freitag, M. & Avouris, P. Carrier scattering, mobilities, and electrostatic potential in monolayer, bilayer, and trilayer graphene. *Phys. Rev. B* **80,** 235402 (2009).
10. Dresselhaus, M. S. & Dresselhaus, G. Intercalation compounds of graphite. *Adv. Phys.* **51,** 1–186 (2002).
11. Li, G. & Andrei, E. Y. Observation of Landau levels of Dirac fermions in graphite. *Nature Phys.* **3,** 623–627 (2007).
12. Niimi, Y., Kambara, H. & Fukuyama, H. Localized distributions of quasi-two-dimensional electronic states near defects artificially created at graphite surfaces in magnetic fields. *Phys. Rev. Lett.* **102,** 026803 (2009).
13. Miller, D. L. *et al.* Observing the quantization of zero mass carriers in graphene. *Science* **324,** 924–927 (2009).
14. McCann, E. & Fal'ko, V. L. Landau-level degeneracy and quantum Hall effect in a graphite bilayer. *Phys. Rev. Lett.* **96,** 086805 (2006).
15. Taniguchi, T. & Watanabe, K. Synthesis of high-purity boron nitride single crystals under high pressure by using Ba–Bn solvent. *J. Cryst. Growth* **303,** 525–529 (2007).
16. Dean, C. R. *et al.* Boron nitride substrates for high-quality graphene electronics. *Nature Nanotech.* **5,** 722–726 (2010).
17. Bao, W. *et al.* Magnetoconductance oscillations and evidence for fractional quantum Hall states in suspended bilayer and trilayer graphene. *Phys. Rev. Lett.* **105,** 246601 (2010).
18. Du, X., Skachko, I., Barker, A. & Andrei, E. Y. Approaching ballistic transport in suspended graphene. *Nature Nano.* **3,** 491–495 (2008).
19. Bolotin, K. I., Sikes, K. J., Hone, J., Stormer, H. L. & Kim, P. Temperature-dependent transport in suspended graphene. *Phys. Rev. Lett.* **101,** 096802 (2008).
20. Piazza, V. *et al.* First-order phase transitions in a quantum Hall ferromagnet. *Nature* **402,** 638–641 (1999).
21. Zhang, X. C., Faulhaber, D. R. & Jiang, H. W. Multiple phases with the same quantized Hall conductance in a two-subband system. *Phys. Rev. Lett.* **95,** 216801 (2005).
22. Koshino, M. & McCann, E. Trigonal warping and Berry's phase $N\pi$ in ABC-stacked multilayer graphene. *Phys. Rev. B* **80,** 165409 (2009).
23. Koshino, M. & McCann, E. Landau level spectra and the quantum Hall effect of multilayer graphene. *Phys. Rev. B* **83,** 165443 (2011).
24. Zhang, Y. *et al.* Landau-level splitting in graphene in high magnetic fields. *Phys. Rev. Lett.* **96,** 136806 (2006).
25. Checkelsky, J. G., Li, L. & Ong, N. P. Zero-energy state in graphene in a high magnetic field. *Phys. Rev. Lett.* **100,** 206801 (2008).
26. Feldman, B. E., Martin, J. & Yacoby, A. Broken-symmetry states and divergent resistance in suspended bilayer graphene. *Nature Phys.* **5,** 889–893 (2009).
27. Zhao, Y., Cadden-Zimansky, P., Jiang, Z. & Kim, P. Symmetry breaking in the zero-energy Landau level in bilayer graphene. *Phys. Rev. Lett.* **104,** 066801 (2009).
28. Du, X., Skachko, I., Duerr, F., Luican, A. & Andrei, E. Y. Fractional quantum Hall effect and insulating phase of Dirac electrons in graphene. *Nature* **462,** 192–195 (2009).
29. Song, Y. J. *et al.* High-resolution tunnelling spectroscopy of a graphene quartet. *Nature* **467,** 185–189 (2010).

30. Jungwirth, T., Shukla, S. P., Smrčka, L., Shayegan, M. & MacDonald, A. H. Magnetic anisotropy in quantum Hall ferromagnets. *Phys. Rev. Lett.* **81,** 2328–2331 (1998).
31. Ezawa, M. Supersymmetry and unconventional quantum Hall effect in monolayer, bilayer and trilayer graphene. *Physica E* **40,** 269–272 (2007).
32. Koshino, M. & McCann, E. Parity and valley degeneracy in multilayer graphene. *Phys. Rev. B* **81,** 115315 (2010).
33. Moser, J., Barreiro, A. & Bachtold, A. Current-induced cleaning of graphene. *Appl. Phys. Lett.* **91,** 163513 (2007).

Acknowledgements

We thank M. Koshino and E. McCann for discussions and sharing their preliminary work on LLs in Bernal-stacked TLG. We also thank L. Levitov and P. Kim for discussions, A. F. Young for discussions and experimental help on hBN, and J. D. Sanchez-Yamagishi and J. Wang for experimental help. We acknowledge financial support from the Office of Naval Research GATE MURI and a National Science Foundation Career Award. This research has made use of the NSF-funded MIT CMSE and Harvard CNS facilities.

Author contributions

T. Taychatanapat fabricated the samples and carried out the experiments. K.W. and T. Taniguchi synthesized the hBN samples. T. Taychatanapat and P.J-H. carried out the data analysis and co-wrote the paper.

Additional information

The authors declare no competing financial interests. Supplementary information accompanies this paper on www.nature.com/naturephysics. Reprints and permissions information is available online at http://www.nature.com/reprints. Correspondence and requests for materials should be addressed to P.J-H.